

LETTER • OPEN ACCESS

# Interactions between urban vegetation and surface urban heat islands: a case study in the Boston metropolitan region

To cite this article: Eli K Melaas *et al* 2016 *Environ. Res. Lett.* **11** 054020

View the [article online](#) for updates and enhancements.

## Related content

- [Urban heat island impacts on plant phenology: intra-urban variability and response to land cover](#)  
Samuel C Zipper, Jason Schatz, Aditya Singh *et al.*
- [Impact of urbanization on US surface climate](#)  
Lahouari Bounoua, Ping Zhang, Georgy Mostovoy *et al.*
- [Impacts of wildfires on interannual trends in land surface phenology: an investigation of the Hayman Fire](#)  
Jianmin Wang and Xiaoyang Zhang

## Recent citations

- [Importance of structural and spectral parameters in modelling the aboveground carbon stock of urban vegetation](#)  
Vincent Wang and Jay Gao
- [Dara V. Gaeva \*et al\*](#)
- [Seasonal patterns of canopy photosynthesis captured by remotely sensed sun-induced fluorescence and vegetation indexes in mid-to-high latitude forests: A cross-platform comparison](#)  
Xinchen Lu *et al*

## Environmental Research Letters



## LETTER

## Interactions between urban vegetation and surface urban heat islands: a case study in the Boston metropolitan region

## OPEN ACCESS

RECEIVED  
16 January 2016REVISED  
4 May 2016ACCEPTED FOR PUBLICATION  
5 May 2016PUBLISHED  
19 May 2016

Eli K Melaas, Jonathan A Wang, David L Miller and Mark A Friedl

Department of Earth and Environment, Boston University, 675 Commonwealth Avenue, Boston, MA 02215, USA

E-mail: [emelaas@bu.edu](mailto:emelaas@bu.edu)

Keywords: Landsat, urban heat island, phenology

Supplementary material for this article is available [online](#)

Original content from this work may be used under the terms of the [Creative Commons Attribution 3.0 licence](#).

Any further distribution of this work must maintain attribution to the author(s) and the title of the work, journal citation and DOI.



## Abstract

Many studies have used thermal data from remote sensing to characterize how land use and surface properties modify the climate of cities. However, relatively few studies have examined the impact of elevated temperature on ecophysiological processes in urban areas. In this paper, we use time series of Landsat data to characterize and quantify how geographic variation in Boston's surface urban heat island (SUHI) affects the growing season of vegetation in and around the city, and explore how the quality and character of vegetation patches in Boston affect local heat island intensity. Results from this analysis show strong coupling between Boston's SUHI and vegetation phenology at the scale of both individual landscape units and for the region as a whole, with significant detectable signatures in both surface temperature and growing season length extending 15 km from Boston's urban core. On average, land surface temperatures were about 7 °C warmer and the growing season was 18–22 days longer in Boston relative to adjacent rural areas. Within Boston's urban core, patterns of temperature and timing of phenology in areas with higher vegetation amounts (e.g., parks) were similar to those in adjacent rural areas, suggesting that vegetation patches provide an important ecosystem service that offsets the urban heat island at local scales. Local relationships between phenology and temperature were affected by the intensity of urban land use surrounding vegetation patches and possibly by the presence of exotic tree species that are common in urban areas. Results from this analysis show how species composition, land cover configuration, and vegetation patch sizes jointly influence the nature and magnitude of coupling between vegetation phenology and SUHIs, and demonstrate that urban vegetation provides a significant ecosystem service in cities by decreasing the local intensity of SUHIs.

## 1. Introduction

Urban areas occupy a small proportion of the global land surface, but have a large impact on local-to-global environmental systems. At local scales, urban land use modifies the physical and geometric properties of land surfaces relative to natural land cover, which alters surface energy and radiation budgets (Arnfield 2003). In particular, the presence of buildings, roads, and other impervious surfaces increases absorption of shortwave radiation, decreases energy loss via emission of longwave radiation, and reduces evapotranspiration relative to adjacent natural land cover (Oke 1976, Landsberg 1981). As a result, near-surface air temperatures tend to be 0.5 °C–3.0 °C higher than

surrounding rural areas (Bounoua *et al* 2015, Jochner *et al* 2015 and citations therein)—a phenomenon known as the urban heat island (UHI). Within cities, however, trees and other types of vegetation provide significant local cooling via shading and leaf transpiration, and supply additional ecosystem services through carbon sequestration and provision of habitats for flora and fauna (Nowak and Crane 2002, Wilby and Perry 2006, Peters *et al* 2010, Briber *et al* 2013).

Vegetation phenology—the annual cycle of leaf emergence, development, and senescence of leaves (and flowers)—is strongly controlled by temperature in many ecosystems, and is therefore a widely-used diagnostic of climate change impacts on natural ecosystems (Chmielewski and Rötzer 2001, Parmesan and

Yohe 2003). In biomes where temperature is the dominant control on phenology, UHIs have the potential to alter the growing season of vegetation in cities. Indeed, recent studies have demonstrated that UHI's can lead to earlier emergence of leaves and flowers in spring or delayed senescence in fall. For example, Jochner *et al* (2012) used 30 years of ground observations to show that urbanization in three German cities advanced the timing of spring phenophases for nine deciduous species by 2.6–7.6 days between 1980 and 2009. In an earlier study, Rötzer *et al* (2000) found 1.5–4.0 day advances in the timing of urban spring flowering relative to surrounding rural areas for four species in ten European cities.

While these results provide compelling evidence of the impact of UHIs on vegetation phenology, studies based solely on ground observations provide limited information regarding the spatial complexity of phenology in urban areas. Further, comparison of results across ground-based studies is challenging because different studies use different species, methods of analysis, and data collection protocols (Denny *et al* 2014, Gill *et al* 2015). Satellite remote sensing, on the other hand, provides an objective and quantitative means for assessing patterns in land surface phenology—i.e., spatially integrated measurements of seasonal variation in surface properties measured from remote sensing—that can be examined at local-to-global scales (de Beurs and Henebry 2004). Specifically, time series of vegetation indices such as the normalized difference vegetation index (NDVI) and the enhanced vegetation index (EVI) derived from coarse spatial resolution sensors such as AVHRR (1–8 km), SPOT-VEGETATION (1 km) and MODIS (250–500 m) have been widely used to estimate phenological metrics that measure the timing of spring and autumn phenology (Moulin *et al* 1997, White *et al* 2002, Zhang *et al* 2003, Ahl *et al* 2006, Delbart *et al* 2006, Walker *et al* 2015). While observations from AVHRR, MODIS, and SPOT provide high frequency observations over large areas, the relatively coarse spatial resolution of these instruments presents substantial challenges for studies focused on urban areas, which are highly heterogeneous relative to the spatial resolution of these sensors (Jat *et al* 2008). Further, exotic and ornamental species, which are common in cities and often exhibit phenological behavior that is different from that of native species, can affect the observed signature of climate on plant phenology (Jim and Liu 2001, Körner and Basler 2010).

Within this general framework, the goals of this paper are to exploit new remote sensing-based capabilities to quantify and characterize how UHI intensity affects vegetation phenology in the Boston metropolitan area at landscape-scale, and to improve understanding of how spatial variation in land use and land cover control both the intensity of Boston's UHI and its impact on phenology. To do this, we used estimates of phenophase transition dates from a newly

developed method that uses 30 m Landsat data, Landsat-derived land surface temperature (LST) data and maps of impervious surface area (ISA) and tree canopy cover to address three questions: (1) How does the UHI influence spring and autumn phenology across Boston's urban-rural gradient? (2) How does phenology vary within the city of Boston and how much of this spatial variation is explained by local variation in land cover and land use? And, (3) does the nature of land use surrounding vegetation patches affect UHI intensity at local scales? Note that because we use LSTs derived from remote sensing and not air temperatures to measure the intensity of Boston's UHI, hereafter, we refer to this as the surface urban heat island (SUHI).

## 2. Methods

### 2.1. Study region

Our study region includes the Greater Boston metropolitan area (figure 1), encompassing ~12 000 km<sup>2</sup> of residential and commercial land use in and around Boston, with surrounding rural areas composed of northern hardwood and oak/hickory forests inland and woody wetlands along the coast. Elevation in the study region ranges from 0 to 192 m above sea level and the climate is classified as humid continental. Precipitation is uniform throughout the year, but temperatures are highly seasonal with relatively warm summers and cold winters. In response, deciduous vegetation in the region has well-defined phenology that is primarily controlled by temperature (e.g., Richardson *et al* 2006, Friedl *et al* 2014).

### 2.2. Landsat-based phenology detection

We used all available Landsat TM and ETM+ images from the United States Geological Survey with less than 90% cloud cover for two scenes that cover the Greater Boston metropolitan area (Path 12, Rows 30 and 31; see figure 1). Image digital numbers were converted to surface reflectance using the Landsat Ecosystem Disturbance Adaptive Processing System algorithm (Masek *et al* 2006), and observations contaminated by clouds, cloud shadows, and snow and ice were identified and removed using the Fmask algorithm (Zhu and Woodcock 2012). The final data set included a total of 1175 TM and ETM+ images spanning the period from 1984 to 2013.

To map information related to green leaf phenology, we used the Landsat Phenology Algorithm (LPA; Melaas *et al* 2013) to estimate the long-term average and annual day of year associated with leaf emergence (start of spring; SOS) and autumn senescence (end of season; EOS) at 30 m spatial resolution. Because the LPA was originally designed for application over forested areas with relatively dense tree cover (i.e., with relatively high maximum summertime EVI), we incorporated two modifications to support detection

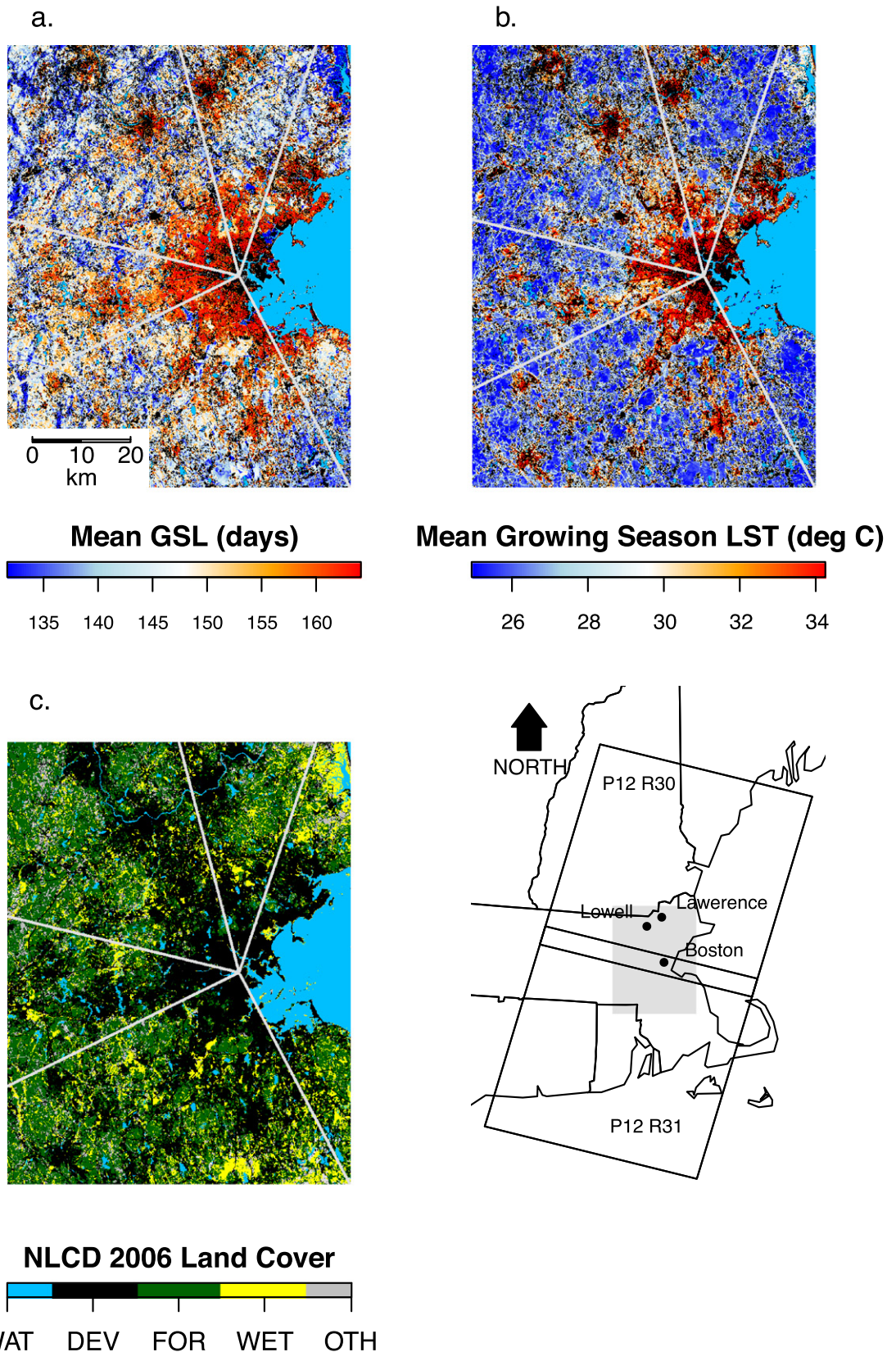
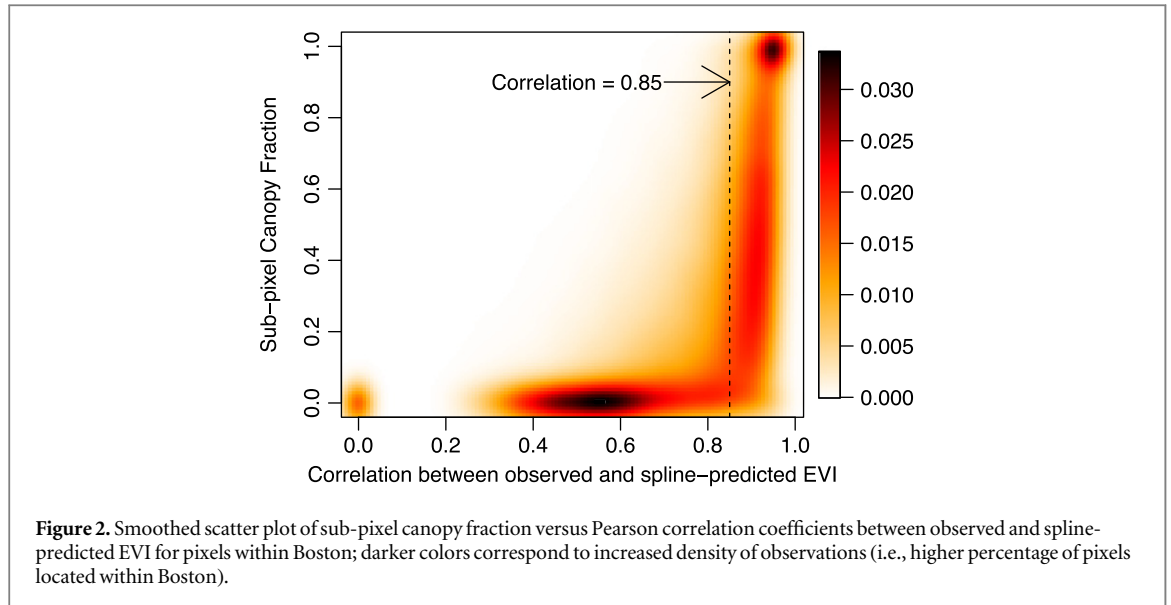


**Figure 1.** (a) Long-term mean growing season length (GSL), (b) long-term mean growing season land surface temperature (LST) and (c) land cover (WAT = water; DEV = developed; FOR = forest; WET = wetlands; OTH = other) maps of the study region. In panels (a) and (b), blue corresponds to water and black corresponds to pixels where the correlation between observed and spline-predicted EVI is less than 0.85. The black boxes in the lower right hand panel are the Landsat TM/ETM+ scenes with corresponding path (P) and row (R) numbers labeled.



of phenology in areas with lower tree cover (i.e., urban areas). First, instead of estimating separate spring and autumn logistic curves to model seasonal variation in Landsat EVI, we used smoothing splines to model the mean annual phenology at each location, and then normalized the resulting function at each pixel to vary between 0 and 1. Similar to Melaas *et al* (2013), the long-term average SOS and EOS at each pixel were estimated based on the date when the normalized spline reached 50% of the spring and autumn amplitude, respectively. Second, using a high-resolution canopy cover map of Boston (see below), we found that arbitrarily defined ranges for long-term mean winter background and peak summer EVI significantly underestimates deciduous tree coverage within the city. Alternatively, since trees are less moisture-limited than grasses and shrubs, they exhibit less interannual variability in summer EVI and, hence, greater agreement (i.e., higher correlation) with a long-term mean fitted cubic spline. Therefore, using the canopy cover map, we identified deciduous forest pixels in our study region where the Pearson correlation between observed EVI values and the fitted cubic spline was greater than 0.85 (figure 2). When the correlation was less than 0.85, the pixel did not consistently follow the relatively stable annual cycle of greenness of deciduous trees, and was assumed to contain mostly grasses and shrubs (e.g. lawns and golf courses) or ISA (see supplementary material).

### 2.3. Landsat-based surface temperature estimation

Remotely sensed SUHI intensity is widely mapped over various scales using land surface temperature (LST; Yuan and Bauer 2007, Peng *et al* 2011). For this work, we converted top-of-atmosphere brightness temperatures from the Landsat TM and ETM+ thermal band to LST for all images between May 1 and

September 1 using a first-order thermal radiative transfer equation:

$$L_{\lambda} = [\varepsilon L_T + (1 - \varepsilon)L_D]\tau + L_U,$$

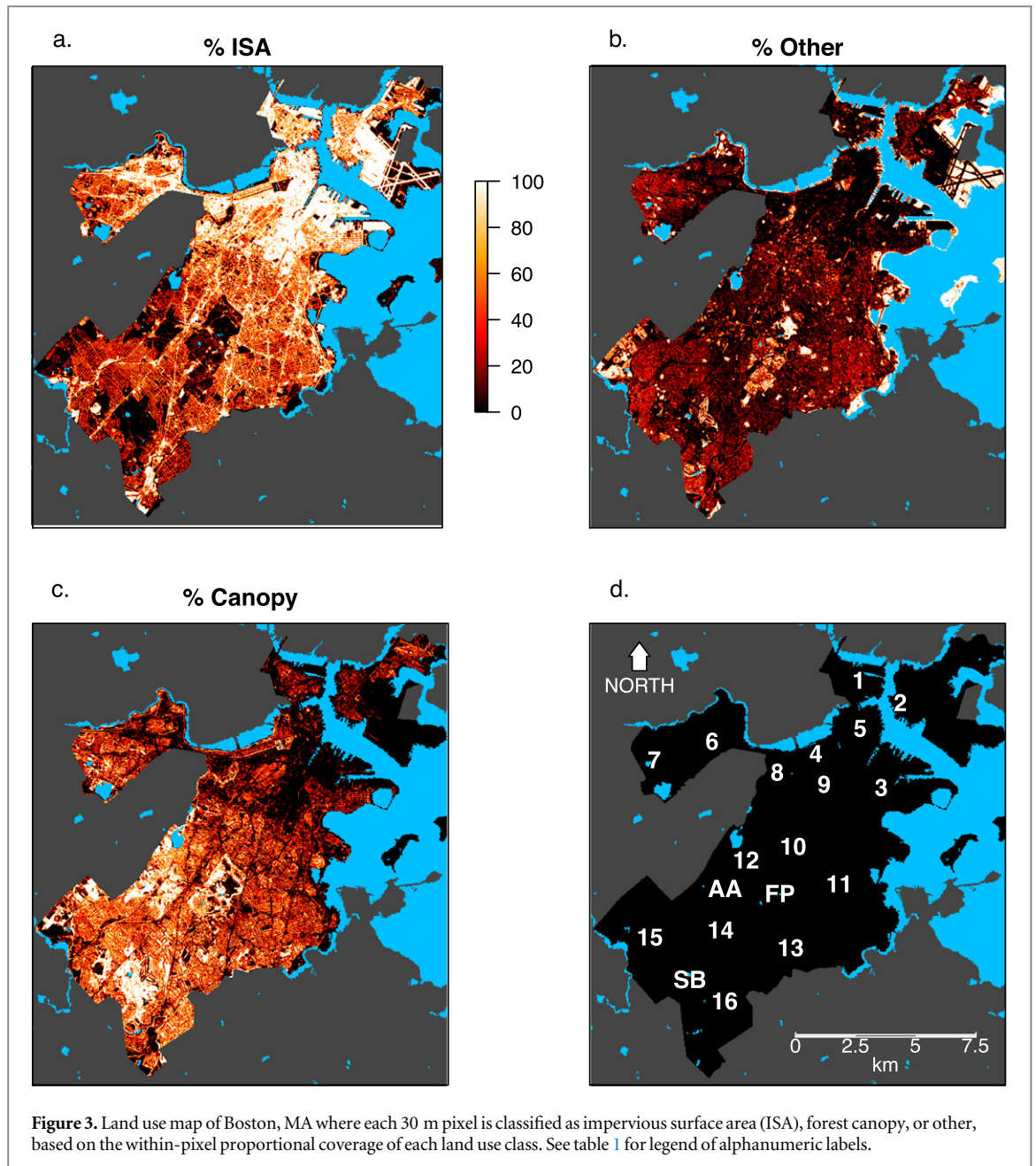
where  $\tau$  is the atmospheric transmissivity,  $\varepsilon$  is the land surface emissivity,  $L_{\lambda}$  is the sensor-detected radiance,  $L_T$  is the target pixel surface radiance, and  $L_D$  and  $L_U$  are the downwelling and upwelling path radiances at the surface and top-of-atmosphere, respectively (Sobrino *et al* 2004). The radiance values ( $L_{\lambda}$  and  $L_T$ ) were converted to brightness temperatures ( $T_b$ ) using sensor-specific Landsat calibration constants and the inverse Planck equation:

$$T_b = \frac{k_2}{\ln\left(\frac{k_1}{L_T} + 1\right)},$$

where  $k_1 = 666.09 \text{ W m}^{-2} \text{ sr}^{-1} \mu\text{m}^{-1}$  and  $k_2 = 1282.71 \text{ K}$  for Landsat 7 ETM+, and  $k_1 = 607.76 \text{ W m}^{-2} \text{ sr}^{-1} \mu\text{m}^{-1}$  and  $k_2 = 1260.56 \text{ K}$  for Landsat 5 TM (Barsi *et al* 2005). Atmospheric correction was performed using an algorithm based on the MODTRAN5 atmospheric radiative transfer model (Barsi *et al* 2005; <http://atmcorr.gsfc.nasa.gov/>), which uses atmospheric profiles of temperature, humidity, and pressure from the National Centers for Environmental Prediction (NCEP) to estimate values for  $\tau$ ,  $L_U$ , and  $L_D$ . We ran MODTRAN at  $42^{\circ} \text{ N}$ ,  $71^{\circ} \text{ W}$  and at 15:16 GMT, which corresponds to the approximate location of Boston and time of the Landsat overpass. Note that because the MODTRAN tool provided by Barsi *et al* (2005) includes NCEP data extending back to 2000, and the LST data used in this analysis includes imagery from 2000 to 2013.

To prescribe the emissivity at each pixel, we computed area-weighted emissivities based on three sub-pixel land cover constituents (vegetation, bare soil, and urban):

$$\varepsilon = f_{\text{urb}}\varepsilon_{\text{urb}} + f_{\text{veg}}\varepsilon_{\text{veg}} + f_{\text{soil}}\varepsilon_{\text{soil}},$$



where the  $f$  subscript denotes the sub-pixel fraction of urban, vegetation, and soil background within each pixel,  $\varepsilon$  is the effective emissivity over the Landsat thermal bandpass, and where values for constituent emissivities ( $\varepsilon_{\text{urb}} = 0.9394$ ,  $\varepsilon_{\text{veg}} = 0.9740$ ,  $\varepsilon_{\text{soil}} = 0.9679$ ) were based on published data (Baldrige *et al* 2009; see supplementary material). Values of fractional urban land cover,  $f_{\text{urb}}$ , were estimated using the Massachusetts Office of Geographic Information's ISA layer (MassGIS 2007), which was generated using 50 cm near infrared orthoimagery and includes all constructed surfaces and man-made compacted soil (i.e., where no vegetation is present). To estimate the fraction of vegetative cover in each pixel,  $f_{\text{veg}}$ , we used an approach similar to that used by Carlson and Ripley (1997) and Sobrino *et al* (2008) (who estimated  $f_{\text{veg}}$  as a function of NDVI), but used EVI because it provides greater dynamic range than the NDVI:

$$f_{\text{veg}} = \left[ \frac{\text{EVI} - \text{EVI}_{\min}}{\text{EVI}_{\max} - \text{EVI}_{\min}} \right]^2,$$

where  $\text{EVI}_{\min}$  ( $=0.123$ ) and  $\text{EVI}_{\max}$  ( $=0.660$ ) were determined using a 1 m spatial resolution map of canopy cover map for Boston (Raciti *et al* 2014). The fraction of bare soil in each pixel,  $f_{\text{soil}}$ , was then calculated as the residual of  $f_{\text{urb}}$  and  $f_{\text{veg}}$ :

$$f_{\text{soil}} = 1 - f_{\text{veg}} - f_{\text{urb}}.$$

This formulation does not include water, which was excluded from the analysis. Further, in contrast to some studies that model sub-pixel cover as a combination of 'high albedo' and 'dark' urban materials (Small 2001, Small and Lu 2006), we assumed that areas located in the  $f_{\text{urb}}$  portion of each pixel were uniform in their emissivity.

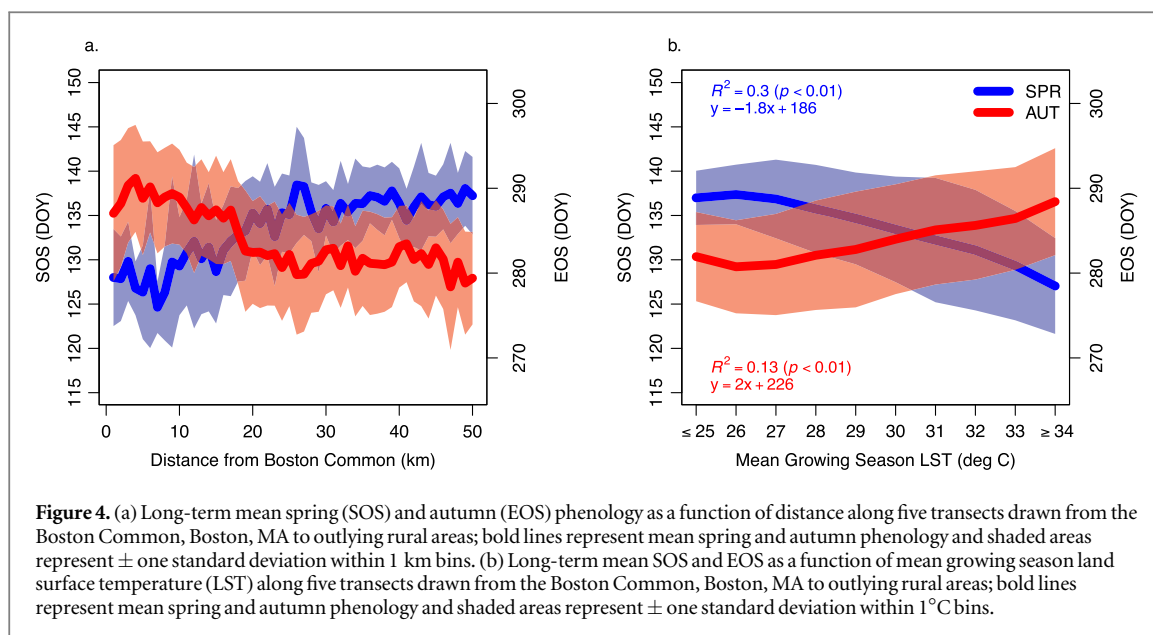


**Table 1.** Legend of notable parks and neighborhoods within Boston listed in figure 3.

Symbol	Neighborhood/Park
1	Charlestown
2	East Boston
3	South Boston
4	Back Bay
5	Downtown
6	Allston
7	Brighton
8	Fenway/Kenmore
9	South End
10	Roxbury
11	Dorchester
12	Jamaica Plain
13	Mattapan
14	Roslindale
15	West Roxbury
16	Hyde Park
AA	Arnold Arboretum
FP	Franklin Park
SB	Stony Brook Reservation

### 2.4. SUHI effect on phenology

Our approach for assessing SUHI impacts on green leaf phenology included two main elements. First, to provide a baseline characterization of SOS and EOS patterns across Boston’s urban-to-rural gradient, we selected five 50 km transects originating at the Boston Common, a forested park in downtown Boston (figure 1). Two transects were located northeast and southeast of Boston (including some coastal areas), two were located inland to the northwest and southwest, and the fifth transect was located west-northwest of the city. Using these transects, we quantified how the timing of mean EOS and SOS vary as function of (1) distance from the city center and (2) average

summertime LST, which we define here as the long-term mean LST based on all available clear-sky observations in May–August (2000–2013).

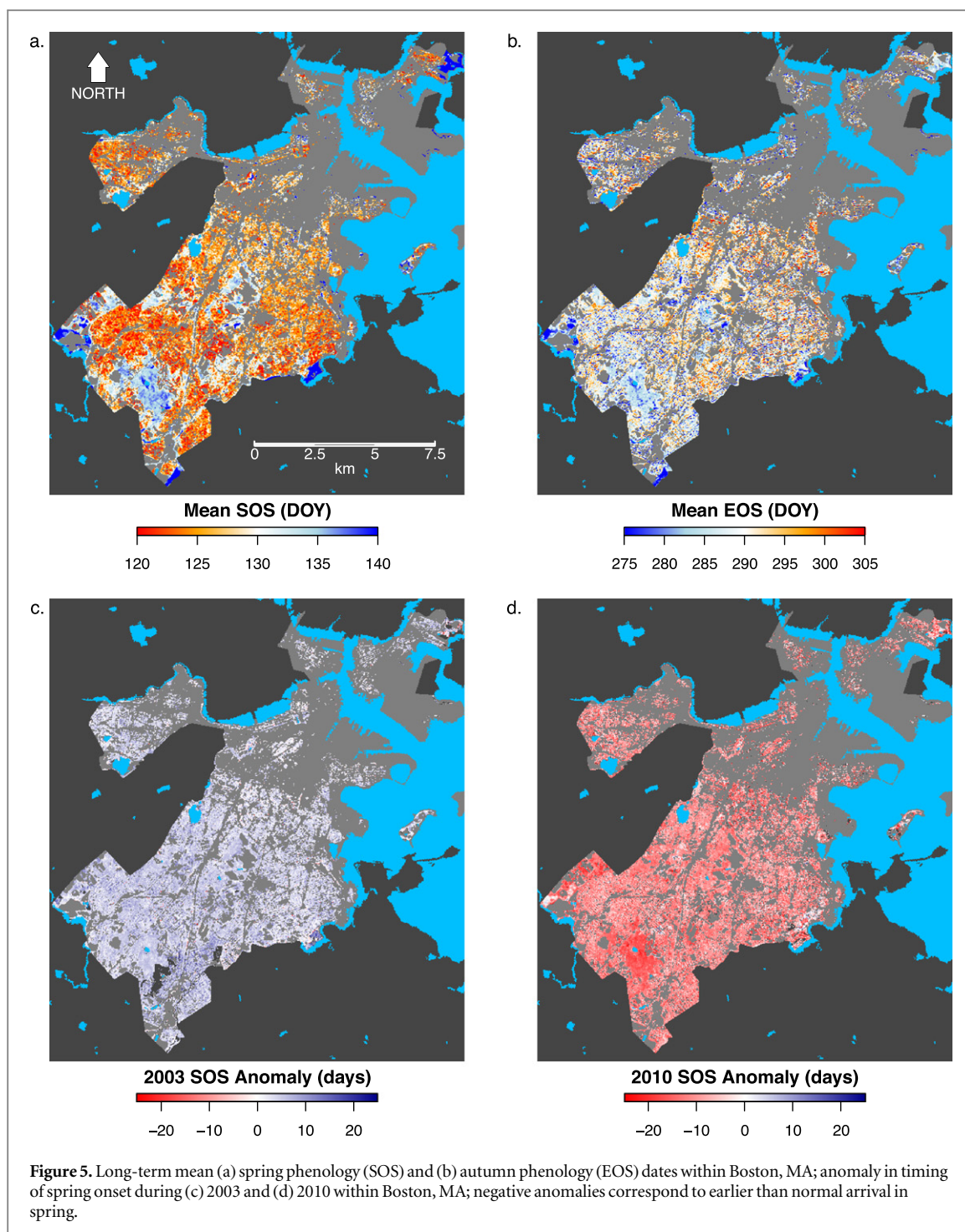
Second, we explored spatial patterns in SOS and EOS within the city of Boston, focusing on land use and vegetation controls. To characterize urban land use and vegetation cover, we estimated the sub-pixel composition of Landsat pixels within Boston’s city limits for each of three surface types: impervious surfaces, tree canopy, and ‘other’ (grasses, wetlands, fields, bare soil etc). To estimate the fractions of ISA and tree canopy cover, we used the high spatial resolution maps of ISA and tree canopy described in section 2.3. The remaining surface area in each pixel was assigned to the ‘other’ class (figure 3). As part of this analysis, we also explored if and how two years with unusually cold and warm springs—2003 and 2010, respectively—affected patterns in SOS and EOS in Boston.

## 3. Results

### 3.1. Phenology along urban-to-rural transects

Results from our analysis show that average growing season length (GSL; EOS–SOS) is approximately 18–22 days longer and mean growing season LST is 7 °C higher in urban areas relative to surrounding rural forests, and that spatial patterns in GSL and LST closely follow land use (figure 1). These relationships are consistent across Boston and in nearby cities (e.g., Lowell and Lawrence, located north of Boston in figure 1(a)). GSL is also significantly shorter for wetlands, most of which are located in coastal areas northeast and southeast of Boston.

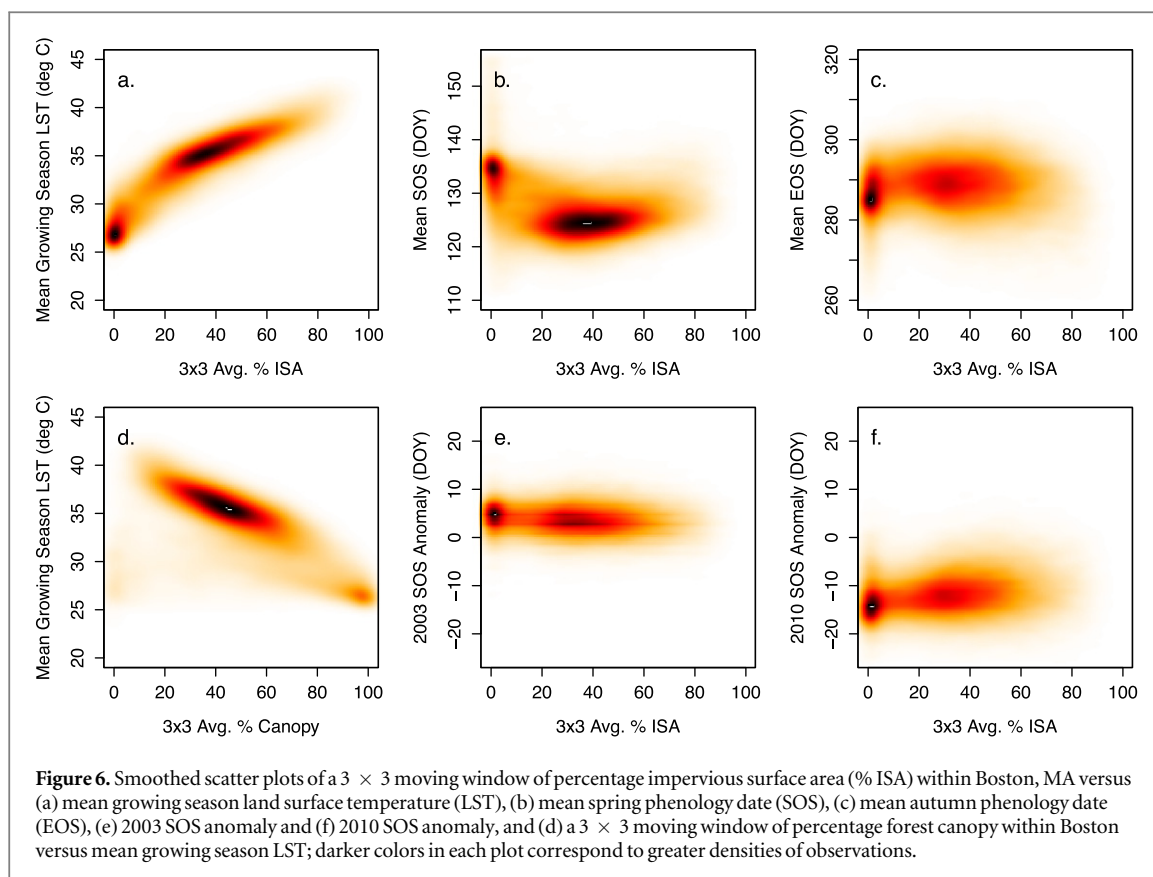
LST and GSL patterns along the five transects in figure 1 show that relative to nearby rural locations,



average SOS occurs about 10–12 days earlier (~May 5) and EOS occurs about 8–10 days later (~October 14) in locations that are within about 15 km of the city center (figure 4(a)). However, patterns in SOS and EOS also show substantial local variation (~4–5 days) caused by heterogeneity in land cover and elevation. In contrast, the relationship between both EOS and SOS as a function of mean growing season LST is smoother (figure 4(b)), but has similar levels of local variation. On average, SOS occurs 1.8 days earlier and EOS occurs 2 days later for each 1 °C increase in mean growing season LST.

### 3.2. Relationships between land use and phenology in Boston

Visual analysis reveals strong complementary gradients in ISA and tree canopy cover between north-eastern and southwestern Boston, with pronounced local variation. Here we focus on fifteen neighborhoods and three green space areas (table 1, figure 3(d)). In the northeast, Charlestown (1), Downtown Boston (5), and East Boston (2) are heavily developed, but include areas with low stature vegetation (grass, shrubs) in parks along the coast and at Logan Airport in East Boston. Densely residential neighborhoods in



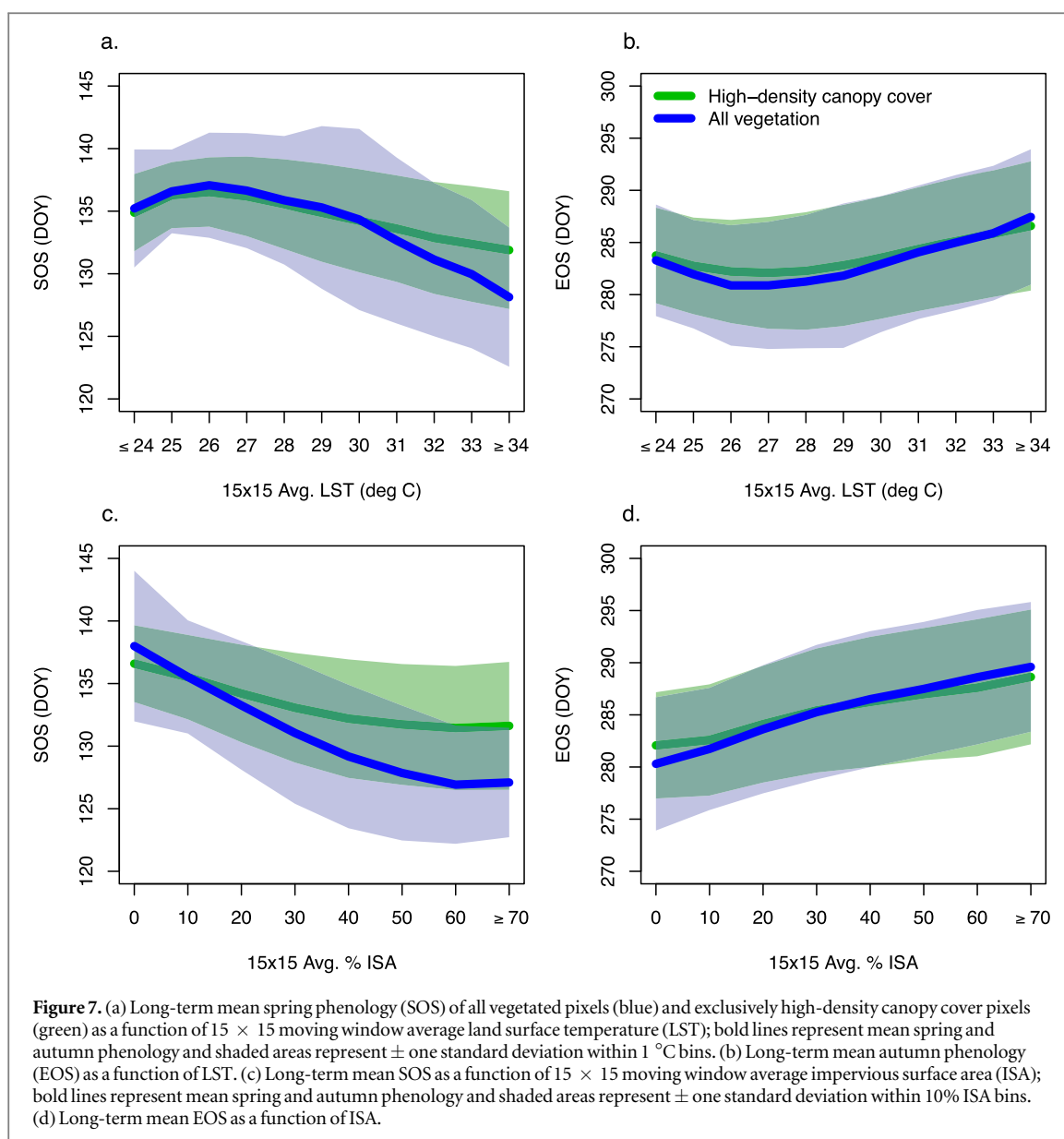
Allston (6), Fenway (8), South Boston (3), and the South End (9) have moderate tree canopy cover and relatively high ISA. Lower density residential neighborhoods have much higher overall tree canopy cover, especially in Hyde Park (16), Jamaica Plain (12), and Roslindale (14).

Long-term mean SOS in Boston ranges from late April to late May (day of year 120–140), and long-term mean EOS ranges from early to late October (day of year 280–290) (figure 5). SOS occurs earlier in neighborhoods such as Jamaica Plain (11) and West Roxbury (15) that have moderate-to-high tree canopy cover mixed with ISA, and later in areas with very dense tree canopy cover such as Franklin Park (FP) and the Stony Brook Reservation (SB). Relative to SOS, spatial patterns in EOS are more variable and show less patch-structure. Spatial variability in both EOS and SOS is highest in neighborhoods such as Dorchester (11) that are the most heterogeneous with respect to tree canopy cover.

SOS across Boston also shows distinct responses to interannual variation in temperatures. In 2003, for example, the average temperature for February, March, and April at Boston Logan International Airport was  $2.9^\circ\text{C}$  below normal (4th coldest on record). In response, SOS anomalies in 2003 were generally positive (i.e., leaves emerged later than normal) by an average of  $4.4 \pm 3.4$  days ( $\pm$  standard deviation; figure 5(c)). In contrast, temperatures during the same period of 2010 were  $4.4^\circ\text{C}$  above normal (3rd

warmest on record) and accumulated growing degree-days were nearly 150% above normal (results not shown). In response, SOS anomalies were uniformly negative (i.e., earlier leaf emergence) by an average of  $10.7 \pm 4.8$  days (figure 5(d)). This effect was most pronounced in areas where average SOS tends to occur later such as the Stony Brook Reservation, where SOS was 15–20 days early in 2010 relative to long-term means.

Finally, to more fully explore the linkage between surface properties and spatial patterns in SOS and EOS, we tested the hypothesis that the amount of ISA in areas surrounding vegetation patches affects local SUHI intensity, and therefore influences the timing of SOS and EOS in urban vegetation patches. Results shown in figure 6(b) appear to confirm this hypothesis: SOS occurs 4.9 days later ( $t(\text{d.f.} = 25\ 580) = 75.4, p < 0.01$ ) in areas surrounded by land cover with less than 20% ISA relative to locations in more developed areas. In autumn, EOS occurs 0.7 days later on average ( $t(\text{d.f.} = 42\ 761) = -12.1, p < 0.01$ ) in areas where ISA is greater than 20%, but the relationship is relatively weak (see, figure 6(c)). In 2003 and 2010, pixels surrounded by areas with higher ISA leafed out about 1 day earlier and 2 days later (respectively) relative to normal (figures 6(e) and (f)), which suggests that the influence of ISA and SUHI on spatial patterns in SOS is weaker in years when spring temperatures are anomalous.



#### 4. Discussion and conclusions

Recent research has suggested that UHIs significantly impact the growing season of vegetation in and around cities (Zhang *et al* 2004, Mimet *et al* 2009, Krehbiel *et al* 2016). Our results support this conclusion, but provide a substantially refined characterization of interactions among urban vegetation cover, UHI intensity and vegetation phenology. At regional scales, results from our analysis demonstrate that spring and autumn phenology vary systematically as a function of distance from the center of Boston (or alternatively, with mean growing season LST), leading to growing seasons that are 18–22 days longer within Boston relative to adjacent rural areas. At any specific location, however, the intensity of Boston's SUHI and the average timing of EOS and SOS are both highly variable and depend on local variation in vegetation cover and land use. Hence, spatial patterns

in both phenology and SUHI in and around Boston form a tightly linked mosaic that is controlled by local variation in land use (ISA) and land cover (vegetation).

More specifically, results from our analyses demonstrate that the amount of ISA surrounding vegetation patches exert complex controls on SUHI and vegetation phenology. At one extreme, locations such as SB and FP have ISA fractions that are close to zero and have growing seasons that are only slightly longer than adjacent rural areas. Examination of the relationship between SUHI and phenology along a continuum of ISA, however, reveals a clear signature of ISA and SUHI on phenology. For example, figure 7 shows how SOS and EOS vary as a function of average ISA across  $15 \times 15$  pixel moving windows for the entire study region. Here, we use the long-term average wintertime and peak summer EVI to identify pixels with low-density canopy cover

and high-density ISA. Pixels with high-density canopy cover have significantly higher average wintertime EVIs (see supplementary material). Using a threshold of wintertime  $EVI \geq 0.15$  and peak summertime  $EVI \geq 0.60$ , we masked out low-density canopy pixels. Using this, we assessed the impact of urbanization on SOS/EOS separately for (1) all vegetated pixels (including street trees) and (2) only high-density canopy pixels. As figure 7 illustrates, the phenology of high-density canopy pixels was less sensitive to urbanization during spring and equally sensitive during autumn. In areas where the  $15 \times 15$  pixel spatial average LST was greater than or equal to  $34^\circ\text{C}$ , the average timing of SOS was 3.8 days later ( $t$  (d.f. = 20 917) =  $-98.6$ ,  $p < 0.01$ ), and in areas where the spatial average ISA greater than or equal to 70%, the average SOS was 4.5 days later ( $t$  (d.f. = 74) =  $-7.6$ ,  $p < 0.01$ ).

Neighborhoods located in Boston's urban core were characterized by higher temperatures, longer growing seasons, and higher proportions of impervious surfaces. In this context, an open question that is not addressed in this paper is the role of species composition in the phenological patterns we observed here. For example, Norway maple (*Acer platanoides*), a non-native species that is widely found in urban areas of Eastern Massachusetts, leafs out earlier and retains its leaves later than most native tree species that in the region (Bertin *et al* 2005). Hence, it is likely that at least part of the pattern in GSL that we attribute to Boston's SUHI is also a reflection of geographic patterns in species composition.

Future climate change is expected to have widespread impacts in urban areas. In Boston, general circulation models project that mean springtime temperatures will rise  $2.4^\circ\text{C}$ – $6.0^\circ\text{C}$  by the end of this century (Kirshen *et al* 2008, McCarthy *et al* 2010). Results presented here show that in 2010, when spring temperatures were approximately  $3^\circ\text{C}$  above average (i.e., at the low end of projected changes), leaf emergence occurred about 10 days earlier than average in Boston, with trees in Boston's largest forested patches leafing out even earlier. These results are consistent with those of Friedl *et al* (2014) and suggest that the growing season of trees and urban forests in New England is likely to shift by as much as 2–4 weeks in the coming decades. The full implications of these changes are unclear, but as the Earth's climate warms and urban areas increasingly respond to climate change, urban ecosystems are likely to experience significant functional and structural changes. From a more practical perspective, results from this study show that urban vegetation has the potential to provide significant societal benefit in cities by reducing the intensity of UHIs (Levis and Bonan 2004).

## Acknowledgments

We thank Lucy Hutyra and Steve Raciti for providing the canopy layer map and Andy Reinmann, Lucy Hutyra, Brady Hardiman and Leah Cheek for helpful comments and suggestions. This work was partially supported by NASA grant numbers NNX12AM82G and NNX14AI70G, and NSF grant numbers DGE-1247312 and EF-1064614. David Miller participated in the Harvard Forest Summer Program in Ecology, which is supported by the NSF BIO REU program. We gratefully acknowledge support from Harvard and the NSF REU program. We also acknowledge the two anonymous reviewers who volunteered their time to review the manuscript.

## References

- Ahl D E, Gower S T, Burrows S N, Shabanov N V, Myneni R B and Knyazikhin Y 2006 Monitoring spring canopy phenology of a deciduous broadleaf forest using MODIS *Remote Sens. Environ.* **104** 88–95
- Arnfield A J 2003 Two decades of urban climate research: a review of turbulence, exchanges of energy and water, and the urban heat island *Int. J. Climatol.* **23** 1–26
- Baldrige A M, Hook S J, Grove C I and Rivera G 2009 The ASTER spectral library version 2.0 *Remote Sens. Environ.* **114** 711–5
- Barsi J A, Schott J R, Palluconi F D and Hook S J 2005 Validation of a web-based atmospheric correction tool for single thermal band instruments *Proc. SPIE* **5882** 58820E1–E7
- Bertin R I, Manner M E, Larrow B F, Cantwell T W and Berstene E M 2005 Norway maple (*Acer platanoides*) and other non-native trees in urban woodlands of central J. *Torrey Bot. Soc.* **132** 225–35
- Bounoua L *et al* 2015 Impact of urbanization on US surface climate *Environ. Res. Lett.* **10** 084010
- Briber B, Hutyra L, Dunn A, Raciti S and Munger J 2013 Variations in atmospheric  $\text{CO}_2$  mixing ratios across a Boston, MA Urban to Rural Gradient *Land* **2** 304–27
- Carlson T N and Ripley D A 1997 On the relation between NDVI, fractional vegetation cover, and leaf area index *Remote Sens. Environ.* **62** 241–52
- Chmielewski F M and Rotzer T 2001 Response of tree phenology to climate change across Europe *Agric. Forest Meteorol.* **108** 101–12
- de Beurs K M and Henebry G M 2004 Land surface phenology, climatic variation, and institutional change: analyzing agricultural land cover change in Kazakhstan *Remote Sens. Environ.* **89** 497–509
- Delbart N, Le Toan T, Kergoat L and Fedotova V 2006 Remote sensing of spring phenology in boreal regions: a free of snow-effect method using NOAA-AVHRR and SPOT-VGT data (1982–2004) *Remote Sens. Environ.* **101** 52–62
- Denny E G *et al* 2014 Standardized phenology monitoring methods to track plant and animal activity for science and resource management applications *Int. J. Biometeorol.* **58** 591–601
- Friedl M A, Gray J M, Melaas E K, Richardson A D, Hufkens K, Keenan T F, Bailey A and O'Keefe J 2014 A tale of two springs: using recent climate anomalies to characterize the sensitivity of temperate forest phenology to climate change *Environ. Res. Lett.* **9** 054006
- Gill A L, Gallinat A S, Sanders-DeMott R, Rigden A J, Short Gianotti D J, Mantooth J A and Templer P H 2015 Changes in autumn senescence in northern hemisphere deciduous trees: a meta-analysis of autumn phenology studies *Ann. Bot.* **116** 875–88
- Jat M K, Garg P K and Khare D 2008 Monitoring and modelling of urban sprawl using remote sensing and GIS techniques *Int. J. App. Earth Obs. Geoinf.* **10** 26–43

- Jim C Y and Liu H T 2001 Species diversity of three major urban forest types in Guangzhou City, China *Forest Ecol. Manage.* **146** 99–114
- Jochner S C and Menzel A 2015 Urban phenological studies: past, present, future *Environ. Pollut.* **203** 250–61
- Jochner S C, Sparks T H, Estrella N and Menzel A 2012 The influence of altitude and urbanisation on trends and mean dates in phenology (1980–2009) *Int. J. Biometeorol.* **56** 387–94
- Kirshen P, Ruth M and Anderson W 2008 Interdependencies of urban climate change impacts and adaptation strategies: a case study of Metropolitan Boston USA *Clim. Change* **86** 105–22
- Körner C and Basler D 2010 Phenology under global warming *Science* **327** 1461–2
- Krehbiel C, Jackson T and Henebry G M 2016 Web-Enabled Landsat Data time series for monitoring urban heat island impacts on land surface phenology *IEEE J. Sel. Topics Appl. Earth Observ. Remote Sens.* **9** 2043–50
- Landsberg H E 1981 *The Urban Climate* (New York: Academic)
- Levis S and Bonan G B 2004 Simulating springtime temperature patterns in the community atmosphere model coupled to the community land model using prognostic leaf area *J. Clim.* **17** 4531–40
- Masek J G, Vermote E F, Saleous N E, Wolfe R, Hall F G, Huemmrich K F, Gao F, Kutler J and Lim T K 2006 A Landsat surface reflectance dataset for North America, 1990–2000 *IEEE Geosci. Remote Sens.* **3** 68–72
- MassGIS Datalayers: Impervious Surface 2007 <http://mass.gov/anf/research-and-tech/it-serv-and-support/application-serv/office-of-geographic-information-massgis/datalayers/imperviousurface.html> (accessed 15 December 2012)
- McCarthy M P, Best M J and Betts R A 2010 Climate change in cities due to global warming and urban effects *Geophys. Res. Lett.* **37** L09705
- Melaas E K, Friedl M A and Zhu Z 2013 Detecting interannual variation in deciduous broadleaf forest phenology using Landsat TM/ETM plus data *Remote Sens. Environ.* **132** 176–85
- Mimet A, Pellissier V, Quenol H, Aguejdad R, Dubreuil V and Roze F 2009 Urbanisation induces early flowering: evidence from *Platanus acerifolia* and *Prunus cerasus* *Int. J. Biometeorol.* **53** 287–98
- Moulin S, Kergoat L, Viovy N and Dedieu G 1997 Global-scale assessment of vegetation phenology using NOAA/AVHRR satellite measurements *J. Clim.* **10** 1154–70
- Nowak D J and Crane D E 2002 Carbon storage and sequestration by urban trees in the USA *Environ. Pollut.* **116** 381–9
- Oke T R 1976 The distinction between canopy and boundary-layer urban heat islands *Atmosphere* **14** 268–77
- Parmesan C and Yohe G 2003 A globally coherent fingerprint of climate change impacts across natural systems *Nature* **421** 37–42
- Peng S, Piao S, Ciais P, Friedlingstein P, Ottle C, Bréon F M, Nan H, Zhou L and Myneni R B 2011 Surface urban heat island across 419 global big cities *Environ. Sci. Technol.* **46** 696–703
- Peters E B, McFadden J P and Montgomery R A 2010 Biological and environmental controls on tree transpiration in a suburban landscape *J. Geophys. Res.—Biogeosci.* **115** G04006
- Raciti S M, Hutya L R and Newell J D 2014 Mapping carbon storage in urban trees with multi-source remote sensing data: relationships between biomass, land use, and demographics in Boston neighborhoods *Sci. Total Environ.* **500** 72–83
- Richardson A D, Bailey A S, Denny E G, Martin C W and O'Keefe J 2006 Phenology of a northern hardwood forest canopy *Glob. Change Biol.* **12** 1174–88
- Rötzer T, Wittenzeller M, Haeckel H and Nekovar J 2000 Phenology in central Europe—differences and trends of spring phenophases in urban and rural areas *Int. J. Biometeorol.* **44** 60–6
- Small C 2001 Estimation of urban vegetation abundance by spectral mixture analysis *Int. J. Remote Sens.* **22** 1305–34
- Small C and Lu J W 2006 Estimation and vicarious validation of urban vegetation abundance by spectral mixture analysis *Remote Sens. Environ.* **100** 441–56
- Sobrino J A, Jiménez-Muñoz J C, Soria G, Romaguera M, Guanter L, Moreno J, Plaza A and Martínez P 2008 Land surface emissivity retrieval from different VNIR and TIR sensors *IEEE Trans. Geosci. Remote* **46** 316–27
- Sobrino J A, Jiménez-Muñoz J C and Paolini L 2004 Land surface temperature retrieval from LANDSAT TM 5 *Remote Sens. Environ.* **90** 434–40
- Walker J J, de Beurs K M and Henebry G M 2015 Land surface phenology along urban to rural gradients in the US Great Plains *Remote Sens. Environ.* **165** 42–52
- White M A, Nemani R R, Thornton P E and Running S W 2002 Satellite evidence of phenological differences between urbanized and rural areas of the eastern United States deciduous broadleaf forest *Ecosystems* **5** 260–73
- Wilby R L and Perry G L W 2006 Climate change, biodiversity and the urban environment: a critical review based on London, UK *Prog. Phys. Geog.* **30** 73–98
- Yuan F and Bauer M E 2007 Comparison of impervious surface area and normalized difference vegetation index as indicators of surface urban heat island effects in Landsat imagery *Remote Sens. Environ.* **106** 375–86
- Zhang X Y, Friedl M A, Schaaf C B, Strahler A H, Hodges J C F, Gao F, Reed B C and Huete A 2003 Monitoring vegetation phenology using MODIS *Remote Sens. Environ.* **84** 471–5
- Zhang X Y, Friedl M A, Schaaf C B, Strahler A H and Schneider A 2004 The footprint of urban climates on vegetation phenology *Geophys. Res. Lett.* **31** L12209
- Zhu Z and Woodcock C E 2012 Object-based cloud and cloud shadow detection in Landsat imagery *Remote Sens. Environ.* **118** 83–94